Original Article

JOURNAL OF THERMOPLASTIC COMPOSITE MATERIALS

Journal of Thermoplastic Composite Materials
2023, Vol. 36(8) 3168–3194

DOI: 10.1177/0892705721122095
journals.sagepub.com/home/jtc
Sage

In-process nip point temperature estimation in automated tape placement based on analytical solution and remote thermal measurements

Anastasios Danezis[1,2], David Williams[2] and Alex A Skordos[1]

Abstract

The optimisation and control of automated tape placement (ATP) requires fast analysis tools able to utilise process data for predictions and monitoring. In this study, a strategy for in-process estimation of nip point temperatures is proposed. The method is based on a combination of two one-dimensional analytical solutions of heat transfer in ATP using temperature data measured on the tool surface, combined with an inverse solution for the estimation of power delivered by the heating device on the composite surface. The performance of the method is examined against a validated finite element model. Approximations of nip point temperature show good correlation for different tool materials, with an average error of 15°C and a maximum of 50°C which is satisfactory for the processing of high-temperature thermoplastic materials. The analytical scheme offers real-time estimations of the nip point temperature with the potential to be used for process control of ATP.

Keywords

process modelling, tape placement, thermoplastic composites, heat transfer analysis, process monitoring, analytical solution

[1]School of Aerospace, Transport and Manufacturing, Cranfield University, Bedford, UK
[2]Heraeus Noblelight Ltd., Cambridge Science Park, Cambridge, UK

Corresponding author:
Anastasios Danezis, School of Aerospace, Transport and Manufacturing, Cranfield University, Building 88, Bedford MK430AL, UK.
Email: a.danezis@cranfield.ac.uk

Introduction

The increasing demand for large composite structures has driven forward the automation of manufacturing methods to overcome low production rates and the variability associated with manual techniques. Automated tape placement (ATP) is an advanced manufacturing process which deploys robotic deposition of tapes onto a tool, building the part in an additive fashion. ATP has gained significant industrial and research interest[1] due to its potential to operate as a single-step process for thermoplastic composites. However, quality on a par with conventional methods is yet to be achieved due to process complexity. Further advancements on the analysis, process monitoring and industrial equipment fronts are necessary to enable the wider adoption of automated methods such as ATP.

Design and optimisation of ATP is a challenging task due to the high number of manufacturing parameters influencing the process and the non-linear heat transfer phenomena involved. Part quality depends strongly on the selection of these parameters, with the influence of temperature history on bond strength development, crystallinity, void content, and thermal degradation playing a critical role.[2–5] These effects have been investigated using heat transfer simulation of ATP, mainly by solving the boundary value problem using numerical methods.[6] Three-dimensional models have been developed,[7-9] but in most cases the domain is reduced to two dimensions assuming uniform heating across the tape width.[10–16] Further simplifications are made by neglecting the heat diffusion in the placement direction based on the dominance of heat transfer due to advection as indicated by the Peclet number.[17,18] In some cases, exo/endo-thermic effects have been included in the analysis,[9–12] while in other cases these have been assumed to be negligible.[13–18] Analytical solutions for the simplified one-dimensional heat transfer problem have been derived.[19–21] In some cases, thermal simulations coupled with material reaction models have been used for process optimisation.[22–24] Surrogate models as well as neural networks and machine learning have been deployed, trained by offline simulation[25–27] or post manufacture data expanded using virtual sample generation methods.[28] Neural networks have been combined with thermal imaging for on-line training and feedback control.[29]

Use of predictive simulation yields results corresponding to ideal process conditions and material properties. Producing zero defect parts with ATP can be facilitated by in-process monitoring to incorporate variations in material behaviour and conditions in process optimisation and control. In the context of ATP, thermography and laser-vision have been used to identify placement and steering defects.[30–33] Optical fibre Bragg grating sensors have also been used to monitor the temperature and strain during placement.[34] These strategies serve an on-line inspection role rather than acting as part of a process control system. Utilisation of thermal measurements in conjunction with inverse methods to identify parameters of the process on-line and project their influence on the product has been put forward in the context of the curing stage of thermosetting composites manufacture.[35,36] Such a development is not currently available for ATP, mainly due to the difficulty of acquiring accurate temperature measurements on the material as it is processed. Thermal imaging is typically used as it allows remote continuous

measurements during placement.[30,31] However, the process nip point and bonding zone are typically out of sight under the compaction roller, and the viewing angle varies with the robot head movements or is limited over convex geometries. Closed-loop control systems based on thermal imaging measure and control temperatures away from the nip point for these reasons; however, significant temperature drop can occur until the material arrives at the nip point due to roller shadowing.[14,17] Embedding sensors in, or in contact with, the moving material is only possible in experimental setups, but not in a production environment due to the additive nature of the process. The concept of a closed-loop control system using thermocouple readings and an approximate process model has been outlined,[19] but its development has not been carried out. Establishing a method for in-process estimation of the temperature at critical locations in the ATP process is a fundamental step in exploiting its automation and high rate potential while meeting product quality requirements.

In this study, a monitoring strategy for ATP of thermoplastic prepregs is put forward based on a combination of 1D heat transfer analytical solutions and temperature data acquired on the tool surface, in contact with the composite substrate, allowing the estimation of nip point temperature in real time. The method integrates an inverse solution to determine the heater power input from the temperature data and enhance the accuracy of nip point estimation. The accuracy of the scheme is assessed against the outputs of a validated 2D finite element model of flashlamp-assisted ATP[17] for a wide range of process rates, number of substrate layers and tool materials. The analytical scheme and inverse solution are also applicable to continuous heating due to the similar bondline temperatures for pulsed and continuous sources of equivalent average power.[17] A virtual processing scenario is studied to showcase the scheme's ability to identify condition changes and highlight the benefits of ATP process monitoring.

Analytical heat transfer approximation of ATP

The 1D analytical approximation combines two solutions describing the two different regimes of heat transfer in ATP. As the part is built up and the thickness increases, the heat transfer shifts from that of a material slab with finite thickness to a semi-infinite body. The transition between the two behaviours is indicated by the Fourier number,[19] which expresses the ratio between conductive heat transport and power storage, with conductive transport being dominant for thin stacks whilst power storage governing heat conduction at high thickness. The Fourier number is

$$F_o = \frac{a_y t}{d^2} \tag{1}$$

where a_y is the thermal diffusivity of the composite in the thickness direction, t is time - in the ATP case the time needed for the tape to reach the nip point after entering the irradiation heating zone - and d is the thickness, which in ATP corresponds to the thickness of material already deposited on the tool.

In tape placement terms, a high Fourier number means that the material thickness is low and/or the process slow enough for a temperature gradient to be established across the thickness direction, whilst a low value implies the deposited material is too thick and/or the process too fast for a significant material depth to be affected by the incoming energy prior to the nip point. The existence of these two heat transfer regimes necessitates two different solutions to approximate conduction effects and a strategy for the transition from one behaviour to the other.

The full ATP heat transfer problem can be reduced to 2D by assuming uniform heating across the tape width and no edge effects.[10–16] In a Eulerian frame attached to the moving placement head, the 2D energy balance coupled with Fourier's heat conduction law is:

$$\rho c_p \left(\frac{\partial T}{\partial t} + u_x \frac{\partial T}{\partial x} + u_y \frac{\partial T}{\partial y} \right) = \dot{q} + \frac{\partial}{\partial x} \left(k_x \frac{\partial T}{\partial x} \right) + \frac{\partial}{\partial y} \left(k_y \frac{\partial T}{\partial y} \right) \tag{2}$$

where T is the temperature, ρ the density, c_p the specific heat capacity, $\dot{q}$ the heat rate, k_x and k_y the conductivities in the longitudinal and thickness direction respectively and u_x, u_y the velocities.

Further simplification of equation (2) can be made as the Peclet number in the placement direction $\left(L_r \rho c_p u_x / k_x\right)$ is very high, indicating that the heat diffusion in the direction of the placement is negligible compared to heat transport due to advection.[17,18] Indeed, for a typical speed of 50 mm/s, longitudinal thermal diffusivity in the $1–10 \times 10^{-6}$ m^2/s range for thermoplastic-based carbon fibre composites and processing length (L_r) as short as the roller diameter, the Peclet number is of the order of 10^3. Low velocities during the first moments of the process can result in low Peclet values; however, this condition holds true for a very short period compared to the duration of the placement. In addition, the longitudinal direction of the material is considered aligned with the material motion so that this principle applies locally to the nip point area where the perpendicular moving tow comes into contact with the substrate. Neglecting the heat diffusion term in the placement direction and aiming for steady state solution, equation (2) results in:

$$\rho c_p \left(u_x \frac{\partial T}{\partial x} + u_y \frac{\partial T}{\partial y} \right) = \dot{q} + \frac{\partial}{\partial y} \left(k_y \frac{\partial T}{\partial y} \right) \tag{3}$$

No material motion takes place in the thickness direction leading to:

$$\rho c_p u_x \frac{\partial T}{\partial x} = \dot{q} + \frac{\partial}{\partial y} \left(k_y \frac{\partial T}{\partial y} \right) \tag{4}$$

The next step of the approximation is to represent the substrate and incoming tow as a single slab which corresponds to the geometry at the nip point section. This material slab is heated at its surface, has a thickness (d) equal to the total thickness of substrate and tow and length (L) equal to the size of the irradiation zone prior to the nip point (Figure 1(b)). The thermal contact resistance between the two composites is assumed to be negligible although its effect has been found to be relevant.[37]

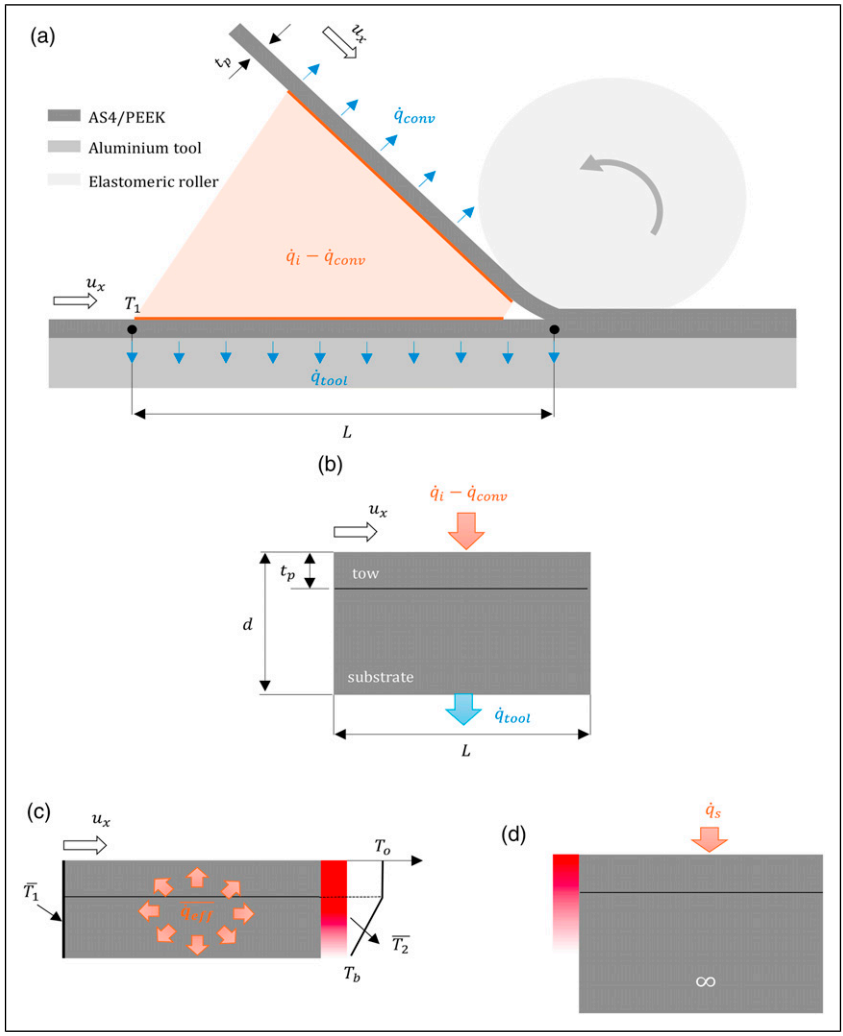

Figure 1. Heat transfer in ATP: (a) 2D representation; (b) simplification of geometry to a single material slab; (c) finite slab behaviour with averaged volumetric heating for Fo>1; (d) semi-infinite body behaviour under surface heating at greater thickness (Fo<1).

Finite slab approximation

For the finite slab behaviour, assuming the material has a uniform temperature at the start of the irradiation zone and at the nip point, $\overline{T_1}$ and $\overline{T_2}$, equation (4) can be approximated by:

$$\rho c_p u_x \frac{\partial T}{\partial x} - \dot{q}_{eff} = 0 \tag{5}$$

Equation (5) can be integrated in the $[0, L]$ range to obtain:

$$\overline{T_2} = \overline{T_1} + \frac{L\overline{\dot{q}_{eff}}}{\rho c_p u_x} \tag{6}$$

where $\overline{\dot{q}_{eff}}$ is the average volumetric heat rate across the path of the tape ($\overline{\dot{q}_{eff}} = \int_0^L \dot{q}_{eff} dx$) from entry to the nip point.

Equation (6) links the material temperature at the start of the irradiation and at the process nip point. Although the entry temperature in ATP is typically ambient and thus uniform, this is not true for the nip point section where steep through-thickness profiles are developed as a result of the energy delivered on the surface of the material and the low transverse thermal conductivity of the material.[17] To account for this, the temperature profile at the nip point location is assumed to have a bilinear shape as shown in Figure 1(c). The temperature of the first ply is assumed to be constant (T_o). In the rest of the material section, temperature decreases linearly to T_b - the temperature of the tool surface. The nip point is at the interface between the incoming tow and substate at one ply depth (t_p) having a temperature T_o. Calculating the average of the assumed profile yields:

$$\overline{T_2} = T_o \frac{t_p + d}{2d} + T_b \frac{d - t_p}{2d} \tag{7}$$

In the approximation expressed by equations (5)–(7), the energy balance operates using the average temperature of the deposited material through the thickness, while surface heat flux becomes part of the heat rate term ($\dot{q}_{eff}$). The total heat rate per unit volume incorporates contributions from the heating source irradiation ($\dot{q}_i$), latent heat due to matrix transformations ($\dot{q}_{latent}$), natural convection ($\dot{q}_{conv}$) and conduction losses to the tool ($\dot{q}_{tool}$). Expressing these as average heat rates yields:

$$\overline{\dot{q}_{eff}} = \overline{\dot{q}_i} + \overline{\dot{q}_{latent}} + \overline{\dot{q}_{tool}} + \overline{\dot{q}_{conv}} \tag{8}$$

The latent heat term ($\dot{q}_{latent}$) accounts for the heat absorbed and released during material transformations of the thermoplastic matrix as well as any other enthalpy changes that may occur. It is assumed negligible compared to the power input of the heating source[13–18] due to the low crystallinity levels typically achieved with ATP and the polymer mass fraction of 30–35%.

The average power losses per unit volume of material due to contact with the tool can be approximated as the average heat transfer by conduction between the lower surface of the first ply and the lower surface of the material slab, assuming a linear increase of T_o and T_b across the irradiation length:

$$\overline{\dot{q}_{tool}} = -k_y \frac{T_o - T_b}{d - t_p} \frac{1}{2d} \tag{9}$$

Similarly, the power losses to air per unit volume due to convection can be approximated as:

$$\overline{\dot{q}_{conv}} = -h\left(\frac{\overline{T_1} + T_o}{2} - T_a\right)\frac{2}{d} \tag{10}$$

where T_a is the ambient temperature and h the natural air convection coefficient. A factor of two is used to account for the two surfaces (deposited material and incoming tow) exposed to air convection.

The average volumetric power input due to radiative heating is:

$$\overline{\dot{q}_i} = \overline{E}_i\frac{1}{d} \tag{11}$$

where $\overline{E}_i$ denotes the average irradiance over the surface of material exposed to radiation.

Combining equations (9)–(11), the total heat rate per unit volume of material is:

$$\overline{\dot{q}_{eff}} = \overline{E}_i\frac{1}{d} - k_y\frac{T_o - T_b}{d - t_p}\frac{1}{2d} - h\left(\frac{\overline{T_1} + T_o}{2} - T_a\right)\frac{2}{d} \tag{12}$$

Combination of equations (6), (7) and (12) yields:

$$T_o = \frac{2\,d\rho c_p u_x\overline{T_1} + 2\overline{E}_i L + hL\left(4\,T_a - 2\overline{T_1}\right) + \left[\frac{k_y L}{d-t_p} - \rho c_p u_x\left(d - t_p\right)\right]T_b}{\rho c_p u_x\left(d + t_p\right) + \frac{k_y L}{d-t_p} + 2hL} \tag{13}$$

which expresses an approximation of the nip point temperature (T_o) based on the measured tool temperature (T_b), the power input ($\overline{E}_i$) and the thermal/geometrical properties of the deposited material.

Semi-infinite body approximation

As the substrate thickness increases the heat transfer phenomena approach the behaviour of a semi-infinite solid with a heat flux ($\dot{q}_s$) applied to its surface (Figure 1(d)). In this regime the temperature at the tool surface is not affected by the irradiation on the surface of the deposited substrate, as the times involved are too short for the heating to propagate through the thickness of the low conductivity material. Using the transformation $x = u_x t$, and taking into account that heat rate due to material transformation is negligible, equation (4) becomes:

$$\rho c_p\frac{\partial T}{\partial t} = \frac{\partial}{\partial y}\left(k_y\frac{\partial T}{\partial y}\right) \tag{14}$$

which for a prescribed surface heat flux has the following established transient semi-infinite body solution[38]:

$$T(y,t) = \overline{T_1} + 2\frac{\dot{q}_s}{k_y}\sqrt{\frac{k_y t}{\pi\rho c_p}}e^{\frac{-y^2\rho c_p}{4k_y t}} + \frac{\overline{\dot{q}_s}}{k_y}y\left(erf\left(\frac{y\sqrt{\rho c_p}}{2\sqrt{k_y t}}\right) - 1\right) \tag{15}$$

Here *erf* is the error function and the average surface flux is:

$$\overline{\dot{q}_s} = \overline{E}_i - 2h\left(\frac{\overline{T_1} + T_o}{2} - T_a\right) \tag{16}$$

obtained similarly to equation (13) for a surface flux instead of volume heating rate.

Combining equations (15), and (16) for the nip point position $(y = t_p)$ and time equal to the travelling across the heating zone (L/u_x) results in:

$$T_o = \frac{\overline{T_1} + \frac{\left(\overline{E}_i + 2hT_a - h\overline{T_1}\right)}{k_y}\left[2\sqrt{\frac{k_y L}{\pi\rho c_p u_x}}e^{\frac{-t_p{}^2\rho c_p u_x}{4k_y L}} + t_p\left(erf\left(\frac{t_p\sqrt{\rho c_p u_x}}{2\sqrt{k_y L}}\right) - 1\right)\right]}{1 + h\left[2\sqrt{\frac{k_y L}{\pi\rho c_p u_x}}e^{\frac{-t_p{}^2\rho c_p u_x}{4k_y L}} + t_p\left(erf\left(\frac{t_p\sqrt{\rho c_p u_x}}{2\sqrt{k_y L}}\right) - 1\right)\right]} \tag{17}$$

Transition between behaviours

The approximations represented by equations (13) and (17) are effective for the case of thin and thick composite substrates respectively. The transition between the two behaviours is governed by the instantaneous Fourier number (equation (1)). Switching between these two behaviours can be done predictively by using the Fourier number and setting a threshold value of 1 for the transition. To ensure the transition in behaviour does not cause a discontinuity, a smooth step using the logistic function is selected between the two solutions:

$$T_o = T_o^o + \frac{\left(T_o^\infty - T_o^o\right)}{1 + e^{C(F_o - 1)}} \tag{18}$$

where T_o^o is the approximation corresponding to the thin stack of material calculated using equation (13) and T_o^∞ the approximation corresponding to a semi-infinite stack using equation (17). The breadth of the transition is controlled by the empirical parameter C, with a large C corresponding to a discontinuous transition and a value of zero corresponding to the average of the two approximations.

Inverse estimation of heater power input

A value of average irradiance ($\overline{E}_i$) acting on the ATP cavity is required for the analytical solutions of equation (13) and equation (17). An initial estimate on each tape can be made:

$$\overline{E}_i = \frac{P\,e}{w\,L} \tag{19}$$

where P is the electrical power of the heat source, e the conversion factor from electrical to optical power and w the width of the irradiated area, typically 10–15% wider than the tape. The irradiance estimated by Equation (19) can deviate significantly from the actual value because the conversion factor and irradiation area have high uncertainty. In addition, effective irradiance may vary across regions where the tool geometry alters the angle or distance of the source to the target surface. It is important for the accuracy of the analytical scheme to identify this input power during the process. An inverse calculation scheme is introduced here, using temperature measurements at the tool surface, based on the direct 1D analytical solution of a two-layered body with a semi-infinite substrate, in the case here representing the tool, under a power-law varying surface flux[39]:

$$\dot{q}(y=0,t) = q_o\left(\frac{t}{t_o}\right)^n \tag{20}$$

Using the same transformation and assumptions as those utilised to obtain equation (14) but for the case of the tool incorporated in the model as a semi-infinite body, the temperature at the interface between the composite and the tool, which coincides with the sensor location during the second deposition at $y = t_p$ relative to the substrate surface, is[39]:

$$T(t_p,t) = \overline{T_1} + \frac{q_o L}{k_y}\sqrt{\frac{4k_y t}{\rho c_p {t_p}^2}}\Gamma\left(1+\frac{n}{2}\right)\left(\frac{4t}{t_o}\right)^{\frac{n}{2}}(K+1)\left[i^{n+1}erfc\left(\sqrt{\frac{\rho\, c_p\, {t_p}^2}{4k_y t}}\right) + \sum_{j=1}^{\infty} K^j i^{n+1} erfc\left(\frac{(2j+1)\sqrt{\rho\, c_p {t_p}^2}}{\sqrt{4k_y t}}\right)\right] \tag{21}$$

where $K = \frac{\varepsilon-1}{\varepsilon+1}$ and $\varepsilon = \sqrt{\frac{\rho\, c_p k_y}{\rho' c_p' k_y'}}$ with ρ', c_p' and k_y' denoting the density, specific heat capacity and transverse conductivity of the tool material respectively and Γ is the gamma function.

In general, the irradiance acting on the tapes follows an asymmetric bell shape.[14,17] This can be approximated by a time-varying triangular profile as illustrated in Figure 2, expressed by:

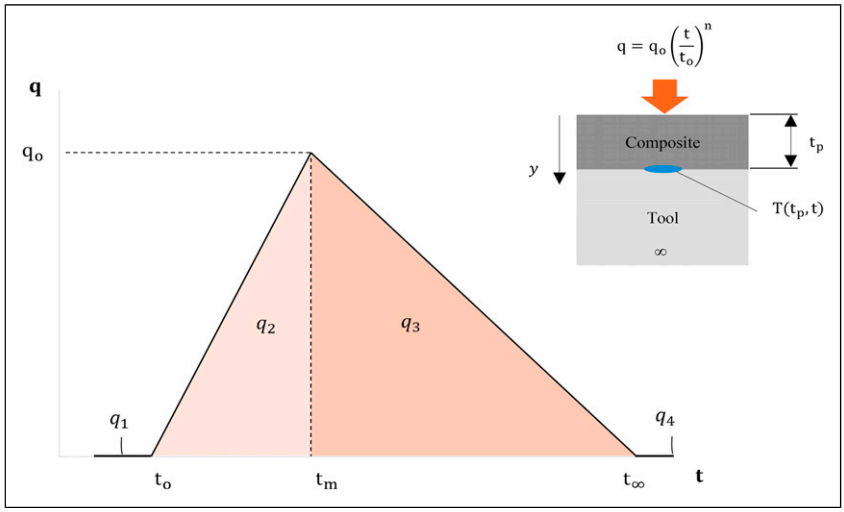

Figure 2. Schematic of the triangular irradiance with the function segments expressed by equation (22), and the configuration of the 1D solution deployed for the inverse scheme.

$$\dot{q}(t,0) = \begin{cases} 0 & t < t_o \\ q_o \dfrac{t - t_o}{t_m - t_o} & t_o \le t \le t_m \\ q_o \dfrac{t_\infty - t}{t_\infty - t_m} & t_m < t \le t_\infty \\ 0 & t \ge t_\infty \end{cases} \tag{22}$$

with q_o representing the peak flux value applied at $t = t_m$, whilst t_o and t_∞ determine the time span of irradiation. Each segment of this heat flux function can be derived from equation (20) with appropriate choice of parameters, and therefore used with equation (21). The interface temperature is the result of the superposition of these segments acting for their corresponding timings. The contribution of each segment is calculated using equation (21) and then the contributions are superimposed to estimate the interface temperature. An initial set of $[q_o, t_o, t_m, t_\infty]$ is needed with an Evolutionary Algorithm in the Solver of Microsoft Excel, which offers a versatile and more efficient implementation compared to other accessible platforms,[40] deployed to identify the optimal set of parameters which satisfies:

$$[q_o, t_o, t_m, t_\infty] = argmin \sum_i \left[T(q_o, t_o, t_m, t_\infty, t_i) - \overline{T}(t_i) \right]^2 \tag{23}$$

where the summation is over all the measured temperature ($\overline{T}$) acquired at times t_i.

The average irradiance acting on the composites inside the ATP cavity is:

$$\overline{E_i} = b\frac{1}{t_\infty - t_o}\int_{t_o}^{t_\infty} q(0,t)\,dt \tag{24}$$

where parameter b accounts for the fact that $\overline{E_i}$ is the average incident irradiance on the substrate and incoming tow, whilst the method identifies only the portion delivered to the substrate. For an equal power distribution between the deposited material and incoming tow the value of b is 2.

The irradiance acting on the tapes is expected to scale linearly with the total power of the heating source whilst changes to the processing rate only rescale the time variable of the distribution. In addition, the irradiance distribution is independent of the inlet temperature and substrate thickness. Therefore, the distribution retrieved with this method corresponds to a placement path and can be used during future depositions across the same path regardless of the changes to these parameters. This method cannot be applied during the first ply deposition as the tool optical properties are different from the tapes, leading to an irradiance distribution not applicable to subsequent processing cycles with a composite substrate.

Strategy for in-process nip point temperature estimation

An overview of the proposed strategy for in-process estimation of nip point temperatures in ATP is illustrated in Figure 3. The manufacturing of the composite part takes place on a tool with a number of sensors strategically placed. The sensors record and feed the controller continuously. Each sensor captures the tool surface temperature (T_b) during the placement of a new layer, which is then used to approximate the nip point temperature at that location using equation (18). The working algorithm uses the position of the placement head to identify the sensor involved and post-process the data. The irradiance value $(\overline{E_i})$ and irradiation length (L) needed are identified during the second ply deposition across the tool geometry via the inverse solution. The rest of the inputs for the remote calculation include the composite thermal properties (c_p, k_y, ρ), processing velocity (u_x), ambient temperature before irradiation $(\overline{T_I})$, thickness of the stack (d) and convection coefficient (h).

Knowledge of the nip point temperature obtained using the approach presented here can allow adjustment of the process conditions through on-line control to maintain its value within an optimal envelope. The processing velocity and heat source power can be adjusted according to the sensitivity of the nip point temperature to these variables. This strategy allows conditions to be adapted as the process progresses and the build-up of thickness alters the heat transfer conditions. Furthermore, potential variability resulting in changes in heat transfer conditions around the part manufactured can be addressed.

Methodology

Predictions from an experimentally validated 2D finite element (FE) model[17] of the placement of AS4/PEEK carbon/thermoplastic tape developed in ANSYS APDL are

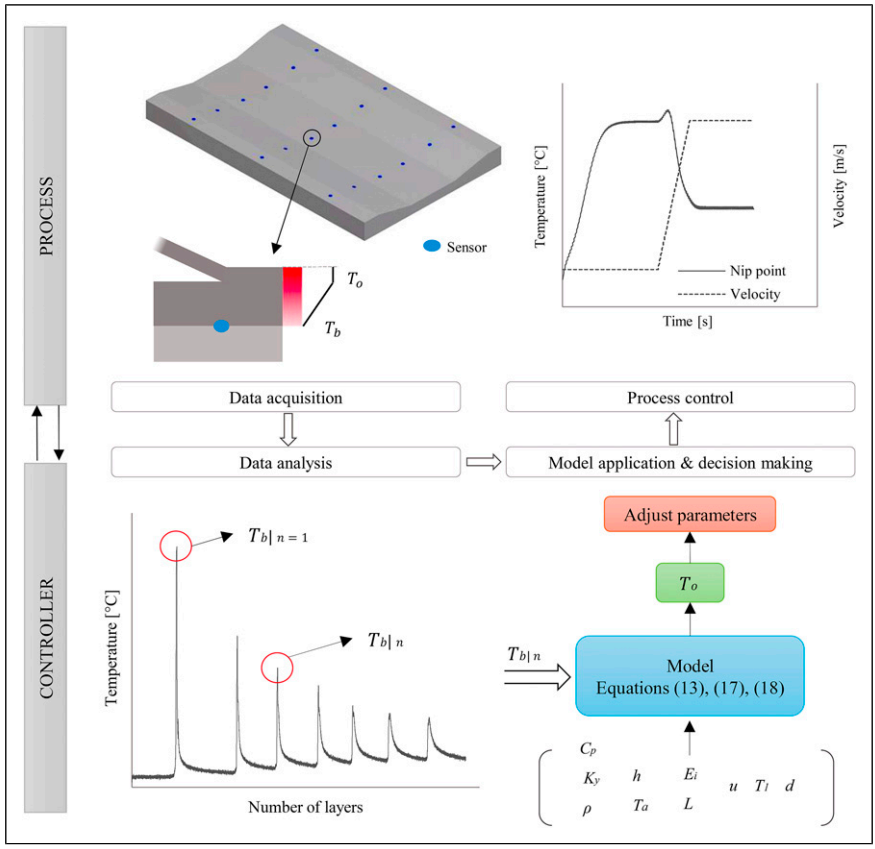

Figure 3. Overview of the strategy for in-process nip point temperature estimation in ATP and utilisation of the modelling estimates for process control.

utilised to examine the performance of the proposed approximation. The process representation includes the incoming tape, deposited material, deformed elastomeric roller, and tool (Figure 1(a)). The incoming tow angle is 45° and the heating zone length (L) is 60 mm. The tool thickness is 15 mm which is sufficient for semi-infinite body behaviour in both cases at the lowest velocity of 25 mm/s and a representative irradiation length of 50 mm. Following the same criterion, the roller of 25 mm radius has been reduced to a 5 mm thin material slice to decrease the number of elements in the analysis. A metallic tool and one made from insulating material are tested to challenge the application of the analytical scheme over a wide range of setups. The thermal properties of the AS4/PEEK composite, roller and different tools are detailed in Table 1. The analytical scheme and inverse solution use average values over the temperature range (Table 1).

An overview of the analytical and FE models is given in Table 2. A Heraeus Noblelight *humm3* system which uses a pulsed Xenon flashlamp of 4.4 kW average electrical power

Table 1. Thermal properties of the AS4/PEEK composite, roller and tool used in the analysis.

Material/ Temperature	Specific heat Capacity[41] (J/kg/K)	Transverse thermal conductivity[41] (W/m/K)	Density[42] (kg/m^3)
AS4/PEEK			
0°C	800	0.38	1601
50°C	930	0.44	1598
100°C	1040	0.51	1593
150°C	1260	0.57	1593
200°C	1300	0.64	1586
250°C	1400	0.70	1575
300°C	1550	0.76	1563
350°C	1650	0.68	1537
400°C	1700	0.65	1524
Average	1290	0.6	1570
Metallic tool	950	237	2700
Insulating tool	1500	0.25	1500
Elastomeric roller	1255	0.25	1250

Table 2. Overview of the analytical and FE model comparison.

Model feature/assumption	Analytical scheme		FE model[17]
	Finite slab	*Semi-infinite*	
Equation-Domain	Equation (13)-1D	Equation (17)-1D	Equation (2)- 2D
Conduction in the thickness direction	Bilinear profile (Figure 1(b))	Yes	Yes
Conduction in the placement direction	Negligible		Negligible
Conduction in the width direction	Negligible		Negligible
Latent heat of melting/ crystallisation	Negligible		Negligible
AS4/PEEK thermal properties	Constant (Table 1)		Temperature-dependent (Table 1)
Interlayer contact	Perfect		Perfect
Composite/tool contact	Perfect		Perfect
Radiative heating	Averaged by inverse estimation		Spatial distributions by 3D ray tracing model[17]

acts as a heater. In the FE model, a combined boundary condition of irradiance and convection was applied on the surface of the composite tapes (Figure 1(a)), with the pulsed operation modelled by activating periodically the heat flux term as dictated by the

operating frequency and pulse duration of the lamp. The pulsing conditions were set to 2.25 ms pulses at 50 Hz for this study. The irradiance distributions have been originally determined using a 3D ray tracing model of the system head, reflector and light guide inside the ATP cavity developed in TracePro LC.[17] The distributions have been reduced to a single profile at the tape centre-line and smoothed to eliminate outliers caused by the statistical nature of the solution. The high heat flux acting on the tape surface imposed a fine through-thickness element size of 10 μm near the surface with the rest of the substrate bulk, roller and tool being represented by a coarser mesh in the 10–200 μm range. All boundaries in the model were subjected to convection with a coefficient of 10 W/m^2/K. The entry temperature of the composite tapes and tool in the analysis frame was set to 20°C.

Although the simulation data were generated for a flashlamp-assisted ATP process, similar behaviour is expected under continuous heating. Previous work has shown that the bondline temperatures are similar for pulsing and continuous sources of equivalent average power.[17] In addition, the effect of pulsing on the surface is diminished at one ply depth. As a result, the performance assessment of the analytical scheme and application of the inverse solution carried out for a pulsed source here can be extended to continuous sources.

Results and discussion

Inverse estimation of irradiance

The temperature profiles on the tool surface predicted by the FE model during the second ply deposition at 100 mm/s are plotted in Figure 4 for metallic and insulating tooling.

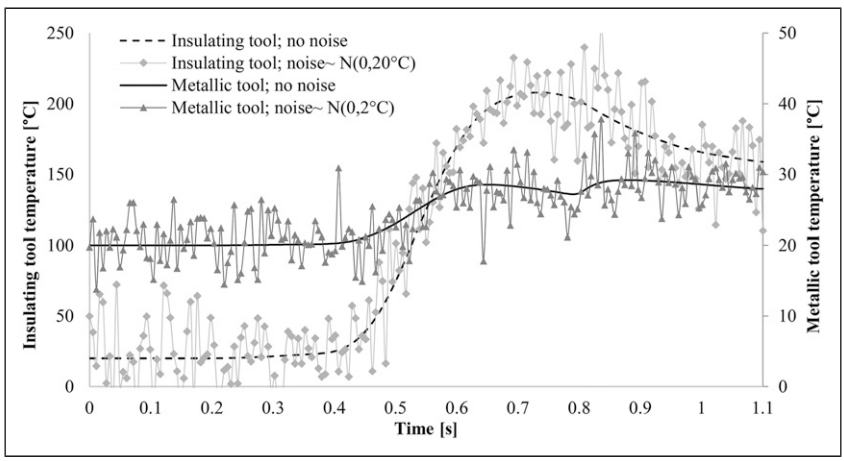

Figure 4. Temperature profiles (FE model) on the tool surface during the 2nd ply deposition at 100 mm/s used for the inverse calculation of irradiance on the substrate surface, before and after the addition of Gaussian noise. Identical independent normally distributed increments with a standard deviation of 2°C for the metallic tool and 20°C for the insulating tool were used to generate the noise superimposed on the FE results.

The profiles correspond to the temperature history of a material point which moves across the 110 mm long analysis frame at the interface between the first ply and the tool. The point enters the irradiation region at 0.2 s at a temperature of 20°C and reaches the nip point at 0.8 s after which a secondary temperature peak occurs due to the additional energy the substrate gains in this case when it comes into contact with the hot incoming tow underneath the roller (0.8–0.94 s). Significantly higher temperatures develop on the surface of the insulating tool during deposition due to its low conductivity which reduces the dissipation of energy. In order to simulate typical noisy temperature sensor data, a Gaussian noise of zero mean value was added to the FE profiles (Figure 4). The standard deviation was set at 2°C for the metallic tool and 20°C for the insulating one, representing approximately 10% of the maximum temperature reached in each case.

The inverse scheme was applied to determine the irradiance input ($\overline{E}_i$). For the parameter estimation in equation (23), an initial value of q_o equal to 8.8×10^5 W/m^2 was used based on equation (19). This value corresponds to half of the available optical power (1.1 kW) delivered to the substrate, assuming equal distribution with the tow and a conversion factor from electrical to optical energy of 0.5, a tape width of 0.025 m and irradiation length of 0.05 m. The selection of initial values for the timing parameters relies on the synchronisation of the robotic head position and sensor data in the process. Here, in order to test the performance of the inverse method under realistic variability, an uncertainty of the temperature sensor position of ±10 mm was assumed which translates to ±0.1 s in the temperature-time data. As a result, the inverse scheme uses temperature data spanning from 0.1 to 0.9 s with the actual time window in the FE model being 0.2–0.8 s. Consequently, t_o =0.1 s, t_∞ =0.9 s and t_m was selected as their mean value at 0.5 s. The value of q_o was constrained in the 10^5–10^6 range whilst the time parameters were constrained to satisfy the inequalities in equation (22).

The values of the triangular profile parameters determined by the inverse solution are reported in Table 3 for the two tool scenarios. For the metallic tool, results based on the original noiseless FE data and for t_∞ fixed at 0.8 s are added to examine the effect of noise and location uncertainty, as well as to showcase the capability of the inverse method to cope with noise in the data. The inversion yields an error of 12% for the metallic tool data with noise and location uncertainty. The contribution of noise to this deviation is about 3%, whilst in the absence of position uncertainty and the same noise levels as previously, an error of 2% over the FE values is accomplished. Consequently, the uncertainty of the nip point timing in the captured temperature profiles has a strong effect on accuracy. Significantly better correlation of the profiles is observed close to the nip point region when t_∞ is known as demonstrated in Figure 5(a). The cases in which t_∞ was assumed equal to 0.9 s and included in the inversion do not follow the FE profile near the nip point accurately. This deviation is caused by the inclusion of temperature data after the nip point in the inversion, as a result of the uncertainty of its exact location. Equation (21) does not describe the behaviour of the secondary temperature peak, which is a result of the heat exchange with the incoming tow, and thus the temperatures calculated are lower in that region with the fitting algorithm compensating with increased irradiance. Changes in the tool material do not affect the accuracy of the inverse solution. The inversion for the insulating tool leads to slightly higher error of 16%, which is attributed to the significant

Table 3. Parameters of the inverse triangular irradiance distribution and comparison of the average with the value applied on the substrate in the FE model. *N* (a,b) denotes a normal distribution with mean a and standard deviation b.

Tool	Noise	t_∞ (s)	q'_o (W/m^2)	t'_o (s)	t'_m (s)	t'_∞ (s)	Average power (W/m^2)	Error %
Insulating	*N* (0, 20°C)	9.0×10^{-1}	4.98×10^5	3.41×10^{-1}	5.05×10^{-1}	8.58×10^{-1}	1.52×10^5	16
Metallic	*N* (0, 2°C)	9.0×10^{-1}	4.41×10^5	3.18×10^{-1}	5.72×10^{-1}	8.58×10^{-1}	1.49×10^5	12
Metallic	*N* (0, 0°C)	9.0×10^{-1}	4.57×10^5	3.51×10^{-1}	5.35×10^{-1}	8.58×10^{-1}	1.45×10^5	9
Metallic	*N* (0, 2°C)	8.0×10^{-1}	4.57×10^5	3.51×10^{-1}	5.35×10^{-1}	8.00×10^{-1}	1.29×10^5	2

noise introduced. The effect of the Gaussian noise on the profile estimation is illustrated in Figure 5(b) for the metallic tool and different realisations of noise using a random number generator and $t_\infty = 0.8$ s. The identified irradiance distribution presents limited variations for the different noise realisations with an average irradiance variability lower than 5%.

Overall, the inverse solution yields satisfactory results even when significant noise is incorporated in the temperature data and sensor position uncertainty exists. The problem of identifying a boundary heat flow based on temperature measured at a depth within the domain is ill-posed.[43] The use of a strong function specification through the triangular profile has a regularising effect on the estimation problem resulting in a robust inversion. Furthermore, the triangular profile is the simplest shape representing the irradiance distribution in ATP and can be expressed in the form of equation (20); and therefore, used in the direct solution of equation (21). The method put forward here obtains an estimate of the irradiance distribution by experimental means with inaccuracy similar to more complicated and time-consuming off-line studies such as optical modelling, whilst also including effects of variability which cannot be considered in off-line computations. The influence of parameters that are either difficult to determine or subject to significant variability, such as the heater efficiency or optical absorptivity, is included in the data captured in real time during the process, and therefore is directly incorporated in the inverse prediction, making the proposed method advantageous compared to off-line predictive strategies.

Nip point temperature determination

Comparison of the FE and analytical predictions of the nip point temperature is presented in Figure 6 for a wide range of process velocities, number of plies and different tool materials, whilst Figure 7 shows a regression plot of the approximate model versus the FE results. The total irradiance used for all analytical calculations corresponds to the case of metallic tooling with 2°C standard deviation noise and $t_\infty = 0.8$ s (Table 3) and was set to 2.58×10^5 W/m^2 assuming an even distribution between substrate and tow $(b = 2)$ and 0.08 m irradiation zone length. The average thermal properties of the composite used are reported in Table 1 and the empirical parameter for the transition to semi-infinite physics (C) in equation (18) was set to 5.

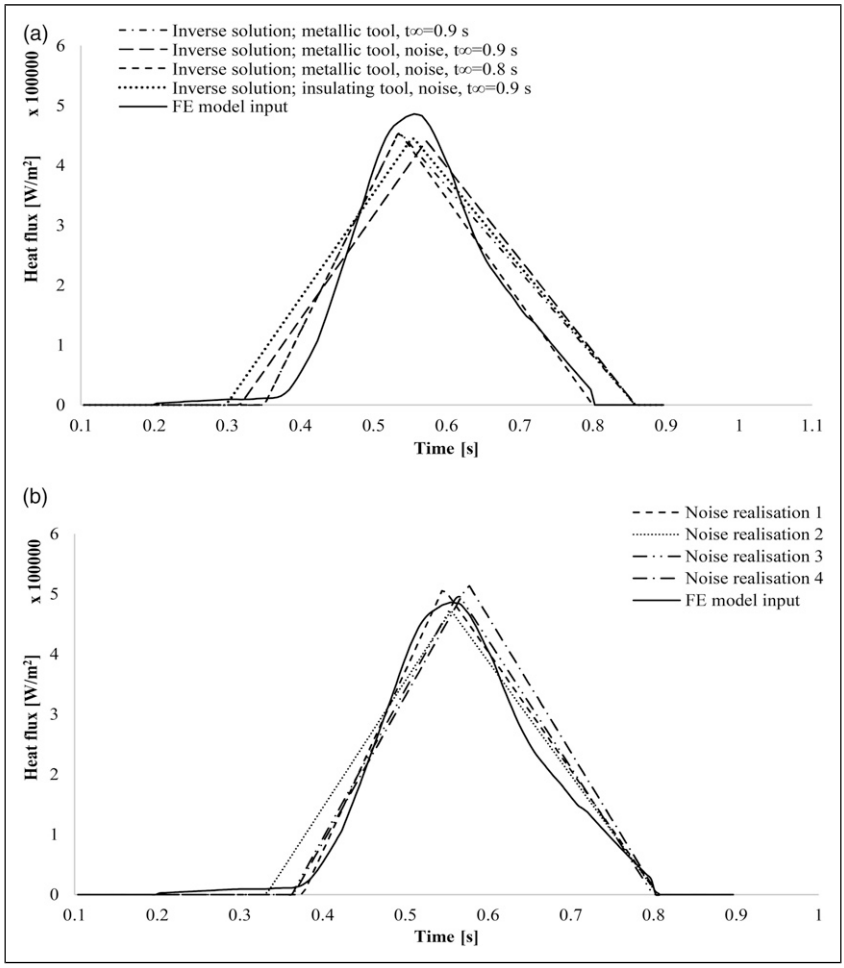

Figure 5. Inverse calculation of irradiance distribution: (a) profiles recovered and the profile applied on the FE model; (b) estimation for different noise realisations for the case of metallic tool, noise of 2°C standard deviation and t∞ fixed at 0.8 s.

Figure 6 shows that the nip point temperature decreases with increasing rate whilst for a given velocity the temperature evolves as the process progresses in a way which depends on the tool material. For the conductive metallic tool (Figure 6(a)), the nip point temperature increases for several layers at the start of the process until it reaches a plateau at which subsequent layer depositions result in similar values. This is caused by the low conductivity of the composite, which reduces heat losses to the tool as its thickness increases, resulting in higher temperature near the surface. The influence of conduction losses towards the tool becomes negligible after a number of layers, depending on the placement velocity. In contrast, the nip point temperature for the insulating tool (Figure 6(b)) decreases for several

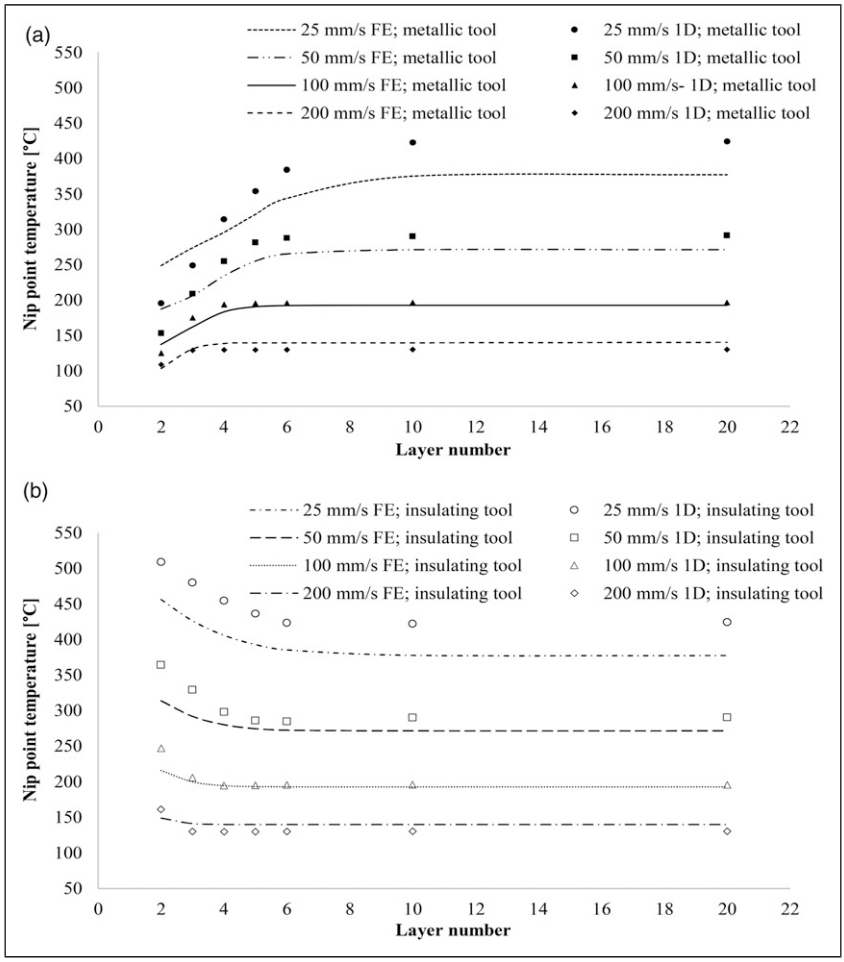

Figure 6. Comparison of the FE and analytical model predictions for a range of velocities, number of layers and: (a) metallic tool; (b) insulating tool.

layers until it converges to the same plateau value as for the metallic tool. The nip point temperatures reached at low thickness are significantly higher compared to the case of highly conductive metallic tooling. In this case, the tool acts as a thermal barrier to heat diffusion resulting in higher nip point values. For the given data, the plateau is reached approximately after the fourth ply at 200 mm/s and the 10^{th} ply at 25 mm/s. This plateau indicates the transition of the heat transfer physics to that of a semi-infinite solid for which an increase of thickness or changes in the tooling material properties do not affect the temperature field. This transition coincides with the reduction of the Fourier number below 1; therefore, it can be predicted, and it is taken in account automatically in the approximation through equation (18). As a result, the predictions for the plateau rely on the semi-infinite

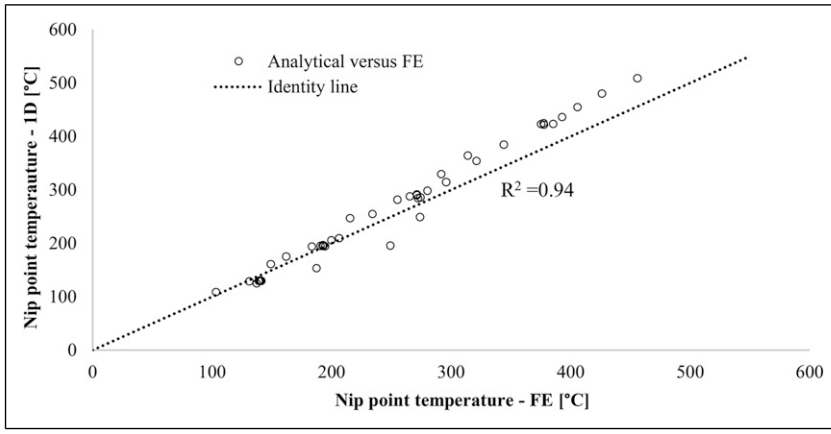

Figure 7. Regression plot of the analytical and FE model predictions indicating good agreement between the two data sets.

solution expressed by equation (17). This transition is also reflected in the tool temperature (T_b) achieved during the deposition and reported in Figure 8. For a given velocity, the tool temperature drops with the number of layers until it becomes virtually equal to ambient for thicknesses similar to those at which the plateau occurs in Figure 6. Only a part of the material near the surface is affected by heating at these thicknesses, indicating conditions of conduction in a semi-infinite solid.

The approximation is in good agreement with the FE results as shown in Figure 7. A linear relation exists between the two sets of predictions which can be approximated by the identity line shown, with a coefficient of determination (R^2) of 0.94. Approximately 85% of the scenarios present an error lower than 30°C whilst 45% of the total data present deviations of less than 10°C. The maximum deviation across all cases is 50°C, encountered in only 4 cases at the lowest speed of 25 mm/s for both tool materials. The deviations at 25 mm/s are high, ranging from 30–50°C, with the analytical scheme mostly overestimating the temperature. This is attributed to the constant thermal properties in the analytical calculations in contrast to the temperature dependence in the FE model. The average conductivity used in the approximation is 0.6 W/m/K for all scenarios, which is applied at a temperature of 180°C (Table 1) in the FE model. The temperatures achieved at 25 and 200 mm/s are up to 400 and 120°C respectively, which correspond to conductivities of 0.65 and 0.52 W/m/K in the FE model. As a result, the analytical predictions correlate well at temperature levels around the value of the average thermal properties and deviate at temperatures away from the average point used. Predictions at 25 mm/s are overestimates whilst predictions at 200 mm/s are underestimates, due to the lower and higher conductivity values used respectively. This can be seen also in Figure 7 where the predictions are in very good agreement below 200°C but gradually start deviating at higher temperatures. The second layer predictions have the highest error. This is attributed to the greater effect of energy losses to the tool during the first depositions, with the

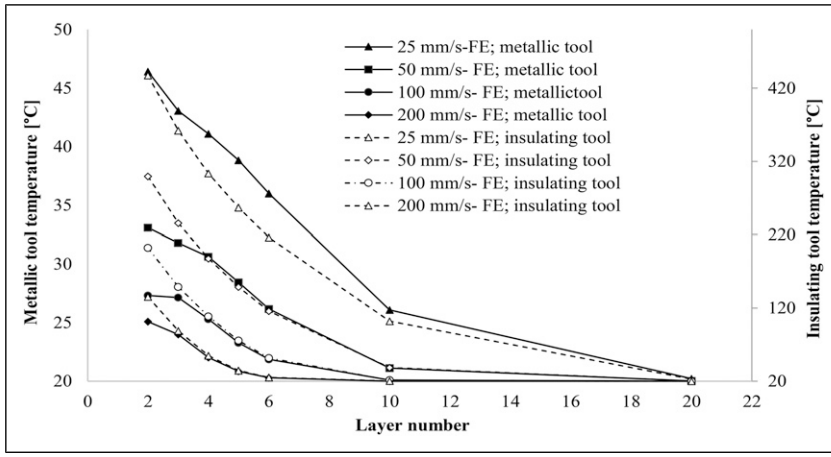

Figure 8. Tool temperature at the nip point section (Tb) given by the FE model used for the analytical calculations.

analytical formulation using a simplified approximation of these. As more layers are added, the influence of the tool is weaker and the heat loss to the tool becomes less important for the nip point prediction. For instance, the second ply deposition for the metallic tool at 50 mm/s presents an error of 34°C whereas for the third layer the error drops to 2°C.

Despite the simplification of the ATP geometry and heat transfer phenomena, the analytical scheme presents good predictive capability for a wide range of process conditions. It can describe the process and follow the nip point temperature evolution regardless of tool material. This is due to the use of a monitoring input in the form of tool temperature (T_b) which compensates for the approximations made. It can also account for increased temperature of the composite prior to the irradiation via the $\overline{T_I}$ input, which in this study was set equal to ambient for all cases. These features render the methodology appealing for application in a manufacturing environment since changes to processing conditions and materials are reflected in the monitoring signals and included in the solution indirectly. This capability offers significant advantages over fully predictive FE analysis that requires a large number of inputs and operates under ideal conditions, whilst it also unlocks the potential for process control. The 15°C average error achieved during the extensive validation of the method is in line with, or an improvement over, thermal imaging which can only capture temperatures outside the consolidation zone. The location of these measurements and the actual nip point are close along the longitudinal direction; however, rapid temperature changes occur in this region as a result of the reduced heater energy reaching deep in the ATP cavity and the abrupt heat exchange when tow and substrate come into contact.[14,17] Furthermore, a constant emissivity value is typically used which can introduce errors when measurements are conducted for the broad temperature range (20–600°C) encountered in ATP.

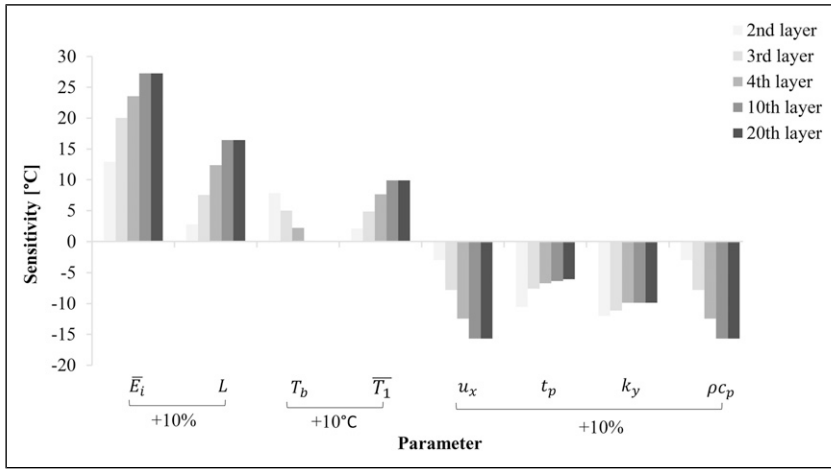

Figure 9. Sensitivity of the analytical scheme inputs to the predicted nip point temperatures for 10%, or 10°C, increase at different layers. Positive sensitivity denotes increase of the nip point value.

Sensitivity of nip point temperature estimation to input parameters

The sensitivity of nip point estimations to the model parameter inputs is presented in Figure 9. The effect of a 10% increase in each variable individually is examined for the baseline scenario of a metallic tool at 50 mm/s process speed. For $\overline{T_1}$ and T_b, a 10°C increment is tested. The convection coefficient and ambient temperature have been excluded due to weak influence. Positive values of sensitivity indicate an increase of nip point temperature under the parameter change examined. Overall, the analytical predictions are highly sensitive to the average irradiance input $(\overline{E_i})$, which increases with the number of layers, reaching a maximum of 27°C temperature increase at high thicknesses. Irradiance is followed in sensitivity by the irradiation length, deposition rate and volumetric heat capacity (ρc_p). Sensitivity to these parameters increases as the process progresses. Tape thickness (t_p) and conductivity (k_y) present an intermediate sensitivity of 10°C which decreases with the placement of new layers. The effect of conductivity becomes weaker as the heat transfer moves towards a semi-infinite state. The sensitivity to inlet temperature $(\overline{T_1})$ increases with the number of plies, whereas that of tool temperature (T_b) decreases towards a zero value. The influence of the latter is strong for only a few layers since thickness and speed allow heat to diffuse to the tool and becomes weak near the transition to a semi-infinite state.

Example application to deposition under varying heater power

The in-process strategy proposed is demonstrated here in a virtual experiment simulated using the FE model. In this scenario, the deposition takes place on an insulating tool, with

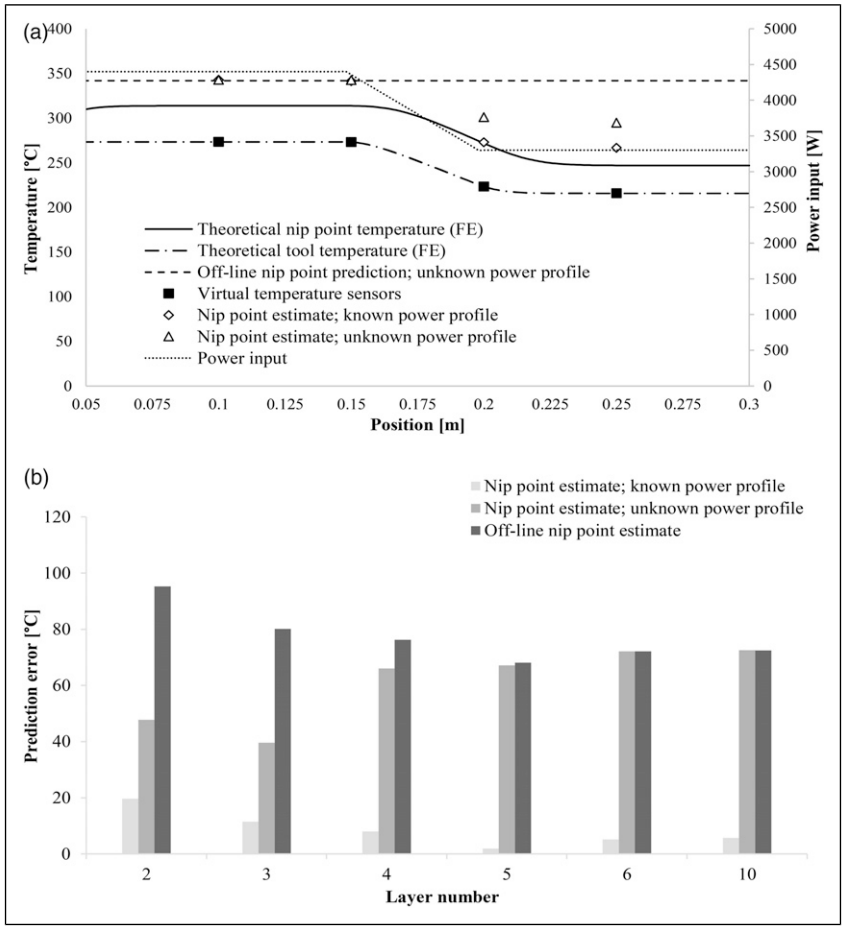

Figure 10. Processing at 50 mm/s with heater power drop: (a) FE profiles and analytical predicitions based on the available information for 2nd ply deposition; (b) errors of nip point temperatures inside the reduced power region for different number of layers.

the properties reported in Table 1, at a speed of 50 mm/s. The tool features four temperature sensors placed 50 mm apart. The irradiance distribution on the tapes is constant across this straight placement path and equivalent to that of Figure 5, with a total irradiance value of 2.58×10^5 W/m^2. During the manufacture, the heater power is reduced to 75% of the initial value, linearly over the span of 1 s as shown in Figure 10(a). Three scenarios are examined that may take place during ATP manufacture: (i) the analytical nip point approximation is carried out knowing a priori the irradiance drop as part of process design; (ii) the power drop is unexpected and needs to be identified by the analytical scheme; (iii) no sensors are used in this tooling region progressing with predictions obtained away from this power variation.

The nip point and tool profiles across the deposited length are plotted in Figure 10(a) for the second layer deposition alongside readings of the virtual sensors. When the power variation is known beforehand, the analytical prediction follows the nip point profile across the processed length satisfactorily, even in the transient region of decreasing power. In the case in which the power variation is not expected, the analytical predictions continue to follow the FE profile closely but with slightly greater error, up to 45°C. The estimation scheme acts in a monitoring sense, identifying the condition changes and potentially allowing their correction in future steps. In the case of solely off-line estimation, the change of nip point temperature is not measured, and predictions are almost 100°C off the theoretical.

The ability of the scheme to follow changes in conditions is also assessed in Figure 10(b) for different number of deposited layers. The analytical predictions inside the reduced-power region are within a 20°C error when the power variations are known. The potential to describe the resulting profile without this knowledge (case of unknown power variation) is good for the first four layers in which the estimation errors are lower than those of off-line studies. However, this capability is lost for thicker substrates due to the low sensitivity of tool temperature, as the heat transfer is shifted to conduction in a semi-infinite solid. The highest errors are obtained in the absence of process monitoring with an error of about 70–100°C.

This example highlights the role monitoring can play in ATP. The scheme allows identification of variations and translates them to changes in nip point temperature. The loss of monitoring capability as the thickness of the component is built up can be partially compensated for by information about the actual power profile obtained during the deposition of the first few layers, using the inverse calculation, which can then be used in a predictive way when the estimation operates in the semi-infinite solid regime.

Conclusions

An analytical approximation consisting of two 1D solutions was developed for estimating the nip point temperatures in ATP based on tool temperature measurements. The solutions address the two heat transfer regimes present in additive processes: heat conduction across a material interface while the deposited material has not reached large thicknesses and heat conduction in a semi-infinite solid governing the behaviour once substantial thickness of material has been built. The scheme is capable of utilising real-time temperature sensor data to estimate the power input profile of the heating source using an inverse solution that has a regularisation behaviour in the presence of significant noise in the temperature signals achieved through function specification of the profile. The nip point predictions assessed against data from a previously validated FE model show good correlation with an average error of 15°C, with the simplification of constant thermal properties and tool losses having the highest impact.

This work puts forward an approach for the heat transfer analysis of ATP which uses process data and simplified models instead of a comprehensive description of the problem requiring numerous high-uncertainty inputs and operating under ideal conditions. The simplicity and computational efficiency of predictions are well suited to in-process control

algorithms. The potential to access approximate values of nip point temperature during the process generates the opportunity to control its value directly, therefore tuning the process to follow temperature profiles optimal in terms of layer bonding and material degradation. Industrial implementation of this approach is expected to trigger further developments, including simplified material transformation models and integration of sensors to supply the scheme with more accurate instantaneous conditions and information about material state. The power input has been addressed here through the inverse solution, but improvements on other critical parameters such as the material thermal properties and stack thickness are necessary, potentially including the effects of partial consolidation and inter-layer thermal resistance on the local effective conductivity.

Acknowledgements

Discussions with Professor Jay I. Frankel of New Mexico State University on the heat flux identification are gratefully acknowledged. Data underlying this study can be accessed through the Cranfield University repository at https://doi.org/10.17862/cranfield.rd.18093260.

Declaration of conflicting interests

The author(s) declared no potential conflicts of interest with respect to the research, authorship, and/or publication of this article.

Funding

The author(s) disclosed receipt of the following financial support for the research, authorship, and/or publication of this article: This work was supported by the Engineering and Physical Sciences Research Council through the EPSRC Centre for Doctoral Training in Composites Manufacture [grant number EP/L015102/1].

ORCID iDs

Anastasios Danezis https://orcid.org/0000-0003-3158-585X
Alex A Skordos https://orcid.org/0000-0003-1273-029X

References

1. Lucaszewicz DHJA, Ward C and Potter KD. The engineering aspects of automated prepreg layup: History, present and future. *Comps B Eng* 2012; 43: 997–1009.
2. Pitchumani R, Ranganathan S, Don RC, et al. Analysis of transport phenomena governing interfacial bonding and void dynamics during thermoplastic tow-placement. *Int J Heat Mass Transf* 1996; 39(9): 1883–1897.
3. Tierney JJ and Gillespie JW, Jr. Crystallization kinetics behavior of PEEK based composites exposed to high heating and cooling rates. *Compos A Appl Sci Manuf* 2004; 35(5): 547–558.
4. Rosselli F, Santare MH and Guceri SI. Effects of processing on laser assisted thermoplastic tape consolidation. *Compos A Appl Sci Manuf* 1997; 28(12): 1023–1033.

5. Khan MA, Mitschang P and Schledjewski R. Parametric study on processing parameters and resulting part quality through thermoplastic tape placement process. *J Compos Mater* 2013; 47(4): 485–499.
6. Orth T, Weimer C, Krahl M, et al. A review of the radiative heating in automated layup and its modelling. *J Plast Technol* 2017; 2(2): 91–125.
7. Chinesta F, Leygue A, Bognet B, et al. First steps towards an advanced simulation of composites manufacturing by automated tape placement. *Int J Mater Form* 2014; 7(1): 81–92.
8. Toso YM, Ermanni P and Poulikakos D. Thermal phenomena in fiber-reinforced thermoplastic tape winding process: computational simulations and experimental validations. *J Compos Mater* 2004; 38(2): 107–135.
9. Schledjewski R and Latrille M. Processing of unidirectional fiber reinforced tapes—fundamentals on the way to a process simulation tool (ProSimFRT). *Compos Sci Technol* 2003; 63(14): 2111–2118.
10. Agarwal V, Guceri SI, McCullough RL, et al. Thermal characterization of the laser-assisted consolidation process. *J Thermoplast Compos Mater* 1992; 5(2): 115–135.
11. Beyeler EP and Guceri SI. Thermal analysis of laser-assisted thermoplastic-matrix composite tape consolidation. *J Heat Transf* 1988; 110(2): 424–430.
12. Sarrazin H and Springer GS. Thermochemical and mechanical aspects of composite tape laying. *J Compos Mater* 1995; 29(14): 1908–1943.
13. Kim HJ, Kim SK and Lee WI. A study on heat transfer during thermoplastic composite tape lay-up process. *Exp Therm Fluid Sci* 1996; 13(4): 408–418.
14. Stokes-Griffin CM and Compston P. A combined optical-thermal model for near-infrared laser heating of thermoplastic composites in an automated tape placement process. *Compos A Appl Sci Manuf* 2015; 75: 104–115.
15. Mantell SC and Springer GS. Manufacturing process models for thermoplastic composites. *J Compos Mater* 1992; 26(16): 2348–2377.
16. Maurer D and Mitschang P. Laser-powered tape placement process–simulation and optimization. *Adv Manuf Polym Compos Sci* 2015; 1(3): 129–137.
17. Danezis A, Williams D, Edwards E, et al. Heat transfer modelling of flashlamp heating for automated tape placement of thermoplastic composites. *Compos A: Appl Sci Manuf* 2021; 145: 106381.
18. Grove SM. Thermal modelling of tape laying with continuous carbon fibre-reinforced thermoplastic. *Composites* 1988; 19(5): 367–375.
19. Weiler T, Emonts M, Wollenburg L, et al. Transient thermal analysis of laser-assisted thermoplastic tape placement at high process speeds by use of analytical solutions. *J Thermoplast Compos Mater* 2017; 31(3): 311–338.
20. Dai SC and Ye L. GF/PP tape winding with on-line consolidation. *J Reinf Plast Compos* 2002; 21(1): 71–90.
21. Ghasemi Nejhad MN, Cope RD and Guceri I. Thermal analysis of in-situ thermoplastic composite tape laying. *J Thermoplast Compos Mater* 1991; 4: 20–45.
22. Sonmez FO and Akbulut M. Process optimization of tape placement for thermoplastic composites. *Compos A Appl Sci Manuf* 2007; 38(9): 2013–2023.

23. Khan MA, Mitschang P and Schledjewski R. Identification of some optimal parameters to achieve higher laminate quality through tape placement process. *Adv Polym Technol* 2010; 29(2): 98–111.
24. Pitchumani R, Gillespie JW, Jr and Lamontia MA. Design and optimization of a thermoplastic tow-placement process with in-situ consolidation. *J Compos Mater* 1997; 31(3): 244–275.
25. Schaefer PM, Gierszewski D, Kollmannsberger A, et al. Analysis and improved process response prediction of laser-assisted automated tape placement with PA-6/carbon tapes using Design of Experiments and numerical simulations. *Compos A Appl Sci Manuf* 2017; 96: 137–146.
26. Heider D, Piovoso MJ and Gillespie JW. A neural network model-based open-loop optimization for the automated thermoplastic composite tow-placement system. *Compos A Appl Sci Manuf* 2003; 34(8): 791–799.
27. Heider D, Piovoso MJ and Gillespie JW, Jr. Application of a neural network to improve an automated thermoplastic tow-placement process. *J Process Control* 2002; 12(1): 101–111.
28. Wanigasekara C, Oromiehie E, Swain A, et al. Machine learning-based inverse predictive model for AFP based thermoplastic composites. . *In. In. Integr* 2021; 22: 100197.
29. Heider D, Piovoso MJ and Gillespie JW, Jr. Intelligent control of the thermoplastic composite tow-placement process. *J Thermoplast Compos Mater* 1998; 11(6): 573–595.
30. Denkena B, Schmidt C, Völtzer K, et al. Thermographic online monitoring system for Automated Fiber Placement processes. *Comps B Eng* 2016; 97: 239–324.
31. Juarez PD and Gregory ED. In-situ thermography of automated fiber placement parts. *Comps B Eng* 2021; 220: 109002.
32. Yadav N, Tranta BO, Schledjewski R, et al. Ply-by-ply inline thermography inspection for thermoplastic automated tape layup. *Adv Manuf Polym Compos Sci* 2021; 7: 49–59.
33. Shadmehri F, Ioachim O, Pahud O, et al. Laser-vision inspection system for automated fiber placement (AFP) process. In: *20th International Conference on Composite Materials*. Copenhagen: July, 2015.
34. Oromiehie E, Prusty BG, Compston P, et al. In-situ simultaneous measurement of strain and temperature in automated fibre placement (AFP) using optical fibre Bragg grating (FBG) sensors. *Adv Manuf Polym Compos Sci* 2017; 3(2): 56.
35. Tifkitsis KI and Skordos AA. Real-time inverse solution of the composites' cure heat transfer problem under uncertainty. *Inverse Probl Sci En* 2020; 28: 1011–1030.
36. Humfeld KD, Gu D, Butler GA, et al. A machine learning framework for real-time inverse modeling and multi-objective process optimization of composites for active manufacturing control. *Comps B Eng* 2021; 223: 109150.
37. Levy A, Heider D, Tierney J, et al. Inter-layer thermal contact resistance evolution with the degree of intimate contact in the processing of thermoplastic composite laminates. *J Compos Mater* 2014; 48(4): 491–503.
38. Azad H, Mustafa MT and Arif A. Analytic solutions of initial-boundary-value problems of transient conduction using symmetries. *Appl Maths Comp* 2009; 215(12): 4132–4140.
39. Cole KB, Beck JV, Woodbury KA, et al. Intrinsic verification and a heat conduction database. *In. . Ther. Sc* 2014; 78: 36–47.

40. Dasović B and Klanšek U. Comparison of spreadsheet-based optimization tools applied to construction site layout problem. *Mat Sci Eng* 2021: 1209.
41. Kim SK, Jung BS, Kim HJ, et al. Inverse estimation of thermophysical properties for anisotropic composite. *Exp Therm Fluid Sci* 2003; 27: 697–704.
42. Cogswell FN. *Thermoplastic Aromatic Polymer Composites*. Oxford: Butterworth Heinemann, 1992.
43. Weber CF. Analysis and solution of the ill-posed inverse heat conduction problem. *Intl J Heat Mass Transf* 1981; 24: 1783–1792.

2022-08-22

In-process nip point temperature estimation in automated tape placement based on analytical solution and remote thermal measurements

Danezis, Anastasios

SAGE

Danezis A, Williams D, Skordos A. (2023) In-process nip point temperature estimation in automated tape placement based on analytical solution and remote thermal measurements. Journal of Thermoplastic Composite Materials, Volume 36, Issue 8, August 2023, pp. 3168-3194
https://doi.org/10.1177/08927057221122095